Volume 12
Number 43
21 November 2021
Pages 14319–14648

Chemical Science

rsc.li/chemical-science

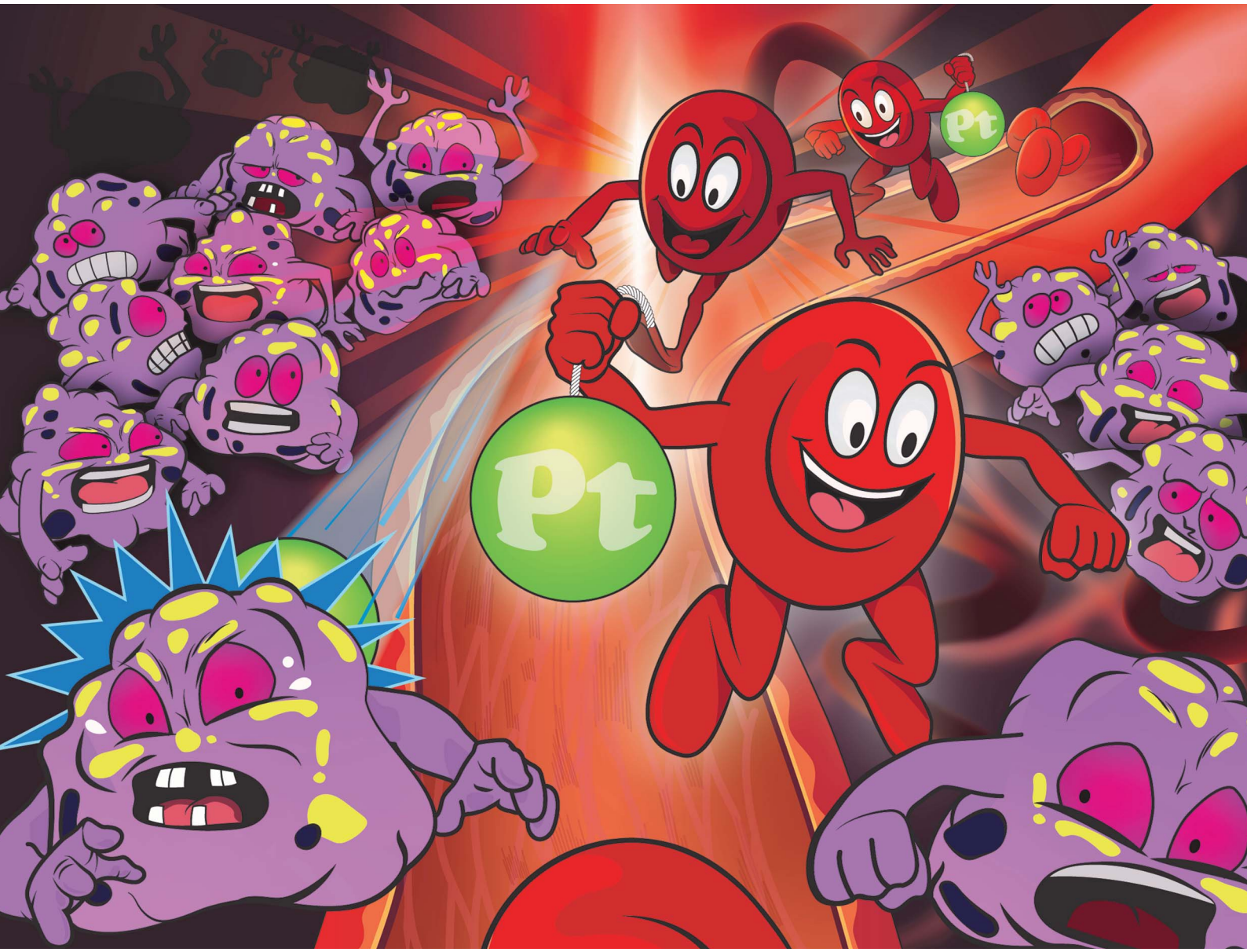

ISSN 2041-6539

ROYAL SOCIETY OF CHEMISTRY

EDGE ARTICLE

Guangyu Zhu *et al.*

An erythrocyte-delivered photoactivatable oxaliplatin nanoprodrug for enhanced antitumor efficacy and immune response

Chemical Science

ROYAL SOCIETY OF CHEMISTRY

EDGE ARTICLE

View Article Online
View Journal | View Issue

Cite this: *Chem. Sci.*, 2021, **12**, 14353

All publication charges for this article have been paid for by the Royal Society of Chemistry

Received 31st May 2021
Accepted 17th September 2021

DOI: 10.1039/d1sc02941j

rsc.li/chemical-science

An erythrocyte-delivered photoactivatable oxaliplatin nanoprodrug for enhanced antitumor efficacy and immune response†

Na Wang,‡[ag] Zhiqin Deng,‡[ag] Qi Zhu,‡[c] Jianxiong Zhao,[c] Kai Xie,[f] Peng Shi,[f] Zhigang Wang,[e] Xianfeng Chen,[d] Feng Wang,[cg] Jiahai Shi[b] and Guangyu Zhu*[ag]

The outcome of conventional platinum (Pt)-based chemotherapy is limited by reduced circulation, failure to accumulate in the tumor, and dose-limiting toxicity arising from non-controllable activation. To address these limitations, we present an erythrocyte-delivered and near-infrared (NIR) photoactivatable Pt^{IV} nanoprodrug for advanced cancer treatment. Compared with small molecule Pt^{IV} prodrugs, this nanoprodrug exhibits significantly enhanced stability, prolonged circulation in the blood, and minimized side effects. The hitchhiking of the nanoprodrug on erythrocytes dramatically increases Pt accumulation in the tumor. Upon irradiation, the nanoprodrug releases oxaliplatin in a controllable manner, resulting in significant antitumor activity against breast tumors *in vivo*, as evidenced by the complete elimination of tumors from a single-dose injection. Additionally, this nanoprodrug is associated with remarkably enhanced immunopotentiation. Our study highlights an efficient strategy to overcome the shortcomings of traditional Pt-based chemotherapy *via* the erythrocyte-mediated delivery of an NIR-activatable nanoprodrug of oxaliplatin, a clinically used anticancer drug.

Introduction

Erythrocytes (*i.e.*, red blood cells) are the main transporters of oxygen to hypoxic organs in mammals.[1] Mature erythrocytes do not contain a nucleus or most organelles, which enables them to deform and pass through narrow capillaries.[2] Erythrocytes have a large surface-to-volume ratio[3,4] and can escape phagocytosis by macrophages by expressing the self-recognition marker CD47 on their surface.[5] In circulation, erythrocytes have a long lifespan of approximately 120 days in humans and 40 days in mice.[5,6] These unique properties make erythrocytes attractive drug carriers.[7–10] The long circulation time facilitates erythrocyte-mediated redistribution of a drug from the plasma to tissues[11,12] and effectively changes the pharmacokinetics.[13,14] Indeed, both donor and autologous erythrocytes have been used for *ex vivo* drug loading and subsequent transfusion into the bloodstream.[15–19] These methods, however, are associated with issues concerning the erythrocyte source and storage and cell damage during the drug encapsulation process.[20,21] Thus, alternative strategies that use intrinsic erythrocytes as autobinding carriers are more desirable.

Recently, Pt^{IV}-based anticancer prodrugs have been studied extensively, with the aim of reducing the side effects and drug resistance associated with the original Pt^{II} anticancer drugs such as oxaliplatin.[22–28] The administration of Pt^{IV} prodrugs, however, still faces significant challenges. For example, small-molecule Pt^{IV} prodrugs may not be stable enough in the circulation system and are also limited by an insufficient circulatory half-life, which reduces Pt accumulation in tumor tissues and thus restricts the drug efficacy.[29,30] Additionally, conventional Pt^{IV} prodrugs do not have the property of controllable activation, leading to adverse effects in off-target tissues.[31] Although small-molecule photoactivatable Pt^{IV} prodrugs have been developed, their activation wavelengths still fall within the visible spectrum and are subject to limited penetration depths.[32–39] Furthermore, although platinum drugs such as oxaliplatin have been reported to induce immunogenic cell

[a]*Department of Chemistry, City University of Hong Kong, Hong Kong SAR, P. R. China. E-mail: guangzhu@cityu.edu.hk*

[b]*Department of Biomedical Sciences, City University of Hong Kong, Hong Kong SAR, P. R. China*

[c]*Department of Materials Science and Engineering, City University of Hong Kong, Hong Kong SAR, P. R. China*

[d]*School of Engineering, Institute for Bioengineering, The University of Edinburgh, Mayfield Road, Edinburgh, EH9 3JL, UK*

[e]*School of Pharmaceutical Sciences, Health Science Center, Shenzhen University, Shenzhen, 518060, P. R. China*

[f]*Department of Biomedical Engineering, City University of Hong Kong, Hong Kong SAR, P. R. China*

[g]*City University of Hong Kong Shenzhen Research Institute, Shenzhen, 518057, P. R. China*

† Electronic supplementary information (ESI) available. See DOI: 10.1039/d1sc02941j

‡ These authors contributed equally to this work.

death (ICD), most of these studies were carried out *in vitro*.[40–42] The prolonged circulation of oxaliplatin may significantly enhance the associated immune response induced *in vivo*. Taken together, a comprehensive study to obtain an NIR-activatable and clinical drug-based Pt^{IV} complex that exhibits enhanced circulation and elicits an elevated immune response *in vivo* is warranted.

To address these challenges, we report the development of an erythrocyte-delivered, NIR-activatable, and multifunctional Pt^{IV} nanoprodrug based on oxaliplatin for advanced cancer therapy. This nanoprodrug exhibited significantly enhanced stability in the blood compared with the small-molecule Pt^{IV} prodrug. Prolonged circulation and enhanced tumor accumulation of the Pt^{IV} nanoprodrug were achieved through auto-binding to erythrocytes in the bloodstream. Following NIR activation of the nanoprodrug, dramatically improved chemotherapeutic outcomes and minimal adverse side effects were observed *in vivo*. Furthermore, an enhanced immune response was observed due to increased drug accumulation in the tumor tissue. To the best of our knowledge, this is the first example of an erythrocyte-delivered and NIR-activatable Pt^{IV} complex based on oxaliplatin, a clinically used Pt-based chemotherapeutic.

Results and discussion

Our anticancer nanoprodrug was designed using the following strategy: to achieve the efficient photoactivation of oxaliplatin-based chemotherapy by NIR, a small-molecule Pt^{IV} prodrug {[Pt(DACH)(PPA)($OCOCH_2CH_2COOH$)(ox)], DACH = (1*R*,2*R*)-1,2-diaminocyclohexane, PPA = pyropheophorbide a, ox = oxalate} that can be activated by red light, designated as PPA-Pt^{IV}-COOH, was first obtained and loaded onto dielectric nanocrystals (NCs). Upon NIR irradiation at 808 nm, where there is minimum water absorption,[43] the NCs can execute energy transfer and emit high-energy visible light at a wavelength of 670 nm, which further photoreduces PPA-Pt^{IV}-COOH and initiates the release of oxaliplatin. This nanocomplex can also achieve an upconversion-mediated photodynamic therapy (PDT) effect due to the presence of the photosensitizer. To achieve intrinsic erythrocyte-mediated delivery, the loaded Pt^{IV} nanocomplex is further functionalized with ERY_1, a peptide with a high affinity for mouse erythrocytes (Scheme 1A).[44] Once the functionalized Pt^{IV} nanoprodrug is in the circulatory system, it will specifically bind to erythrocytes and gradually accumulate in the tumor site, allowing it to kill cancer cells upon irradiation. An increased immune response may also occur due to the accumulation of oxaliplatin and local neoantigens, and the activated immune system may further enhance the antitumor activity of the nanoprodrug.[40,45] As a result, enhanced antitumor efficacy is expected *in vivo*, even with a single-dose intravenous (i.v.) injection (Scheme 1B).

The polyethylenimine (PEI)-capped $NaYbF_4$:Er@$NaYF_4$:Yb/Nd@$NaYF_4$:Ca NCs were first synthesized,[46,47] characterized (Fig. 1A and S1–S3, Table S1†), and verified to be excited at 808 nm to generate upconversion luminescence (UCL) emission at around 670 nm (Fig. 1B). The photoactivatable small-molecule Pt^{IV} prodrug, PPA-Pt^{IV}-COOH (Fig. S4–S9†), was loaded after conjugation with PEI-NCs *via* amine groups. Due to the overlap of the photoluminescence of NCs and the absorption of PPA-Pt^{IV}-COOH (Fig. 1B and C), the generated emission at 670 nm from PEI-NCs may further photoactivate the Pt^{IV} prodrug to release oxaliplatin. The synthesized PPA-Pt^{IV}-NCs were characterized by TEM (Fig. 1D and S10†), and the successful conjugation of PPA-Pt^{IV}-COOH onto PEI-NCs was confirmed by FT-IR, diameter, and zeta potential measurements (Fig. S11 and Table S1†). The loading capacity (LC%, wt%) of the Pt^{IV} prodrug on NCs reached as high as 22% (wt%; Fig. 1E). The photo-controllable drug release property of PPA-Pt^{IV}-NCs was confirmed, and the result clearly indicates that in the presence of a reducing agent, the nanocomplex is quite stable in the dark but can efficiently release oxaliplatin upon NIR irradiation (Fig. S12†). The level of generated $^1O_2$ upon irradiation was also determined.[48] PPA-Pt^{IV}-NCs with the highest loading capacity of 22% displayed a high potency of $^1O_2$ generation (Fig. S13†) and were selected for the following investigations. Such a high drug-loading amount is advantageous for subsequent cancer therapy.

Subsequently, the photocytotoxicity of PPA-Pt^{IV}-NCs was examined in 4T1 (murine breast), MCF-7 (human breast), platinum-sensitive A2780 (human ovarian), and platinum-resistant A2780cisR (human ovarian) cancer cells. A time-dependent cellular accumulation experiment shows that most of the nanocomplex accumulated in the cells after 2 h (Fig. S14†). Thus, this treatment time was selected for further *in vitro* biological tests. The photocytotoxicity of PPA-Pt^{IV}-NCs was examined by a 3-(4,5-dimethyl-2-thiazolyl)-2,5-diphenyl-2-H-tetrazolium bromide (MTT) assay. The cancer cells were treated with various concentrations of PPA-Pt^{IV}-NCs for 2 h in the dark, and then irradiated with an 808 nm continuous-wave (CW) diode laser at a power density of 0.5 W cm^{-2} for 5 min. At this power density, the laser itself had negligible effects on the cell viability (Fig. 1F–I). Without irradiation, the nanocomplex displayed low cytotoxicity in both the cancer cells and MRC-5 normal human lung fibroblasts (Fig. 1J), indicating its biocompatibility. Upon irradiation, PPA-Pt^{IV}-NCs were able to kill cancer cells. For example, the cell viabilities of 4T1 cells treated with 2 μg mL^{-1} PPA-Pt^{IV}-NCs without and with NIR irradiation were 85.3 ± 7.6% and 33.2 ± 4.4%, respectively, showing that PPA-Pt^{IV}-NCs had NIR-controlled cell-killing capability (Fig. 1F). This dramatic photocytotoxicity was also observed in other cell lines (Fig. 1G and H). Remarkably, PPA-Pt^{IV}-NCs showed a strong photocytotoxicity profile in the platinum-resistant A2780cisR cells, in which the cell viability decreased to 4.4 ± 1.6% upon treatment with 2 μg mL^{-1} PPA-Pt^{IV}-NCs (Fig. 1I). The photocytotoxicity of PPA-Pt^{IV}-COOH was also tested (Fig. S15 and S16†). The photocytotoxicity results well substantiate that the as-synthesized PPA-Pt^{IV}-NCs can effectively kill cancer cells upon photoactivation.

We next evaluated the delivery efficiency and photoactivation of our nanocomplex in cancer cells. Compared with the small-molecule Pt^{IV} prodrug, a significantly elevated level of Pt accumulation was observed in the cancer cells after treatment with the nanocomplex. For example, the Pt levels were 41.5 ± 3.1 ng and 851.1 ± 161.7 ng per 10^6 cells after treatment with the same concentration of PPA-Pt^{IV}-COOH and PPA-Pt^{IV}-NCs ([Pt] = 5.7

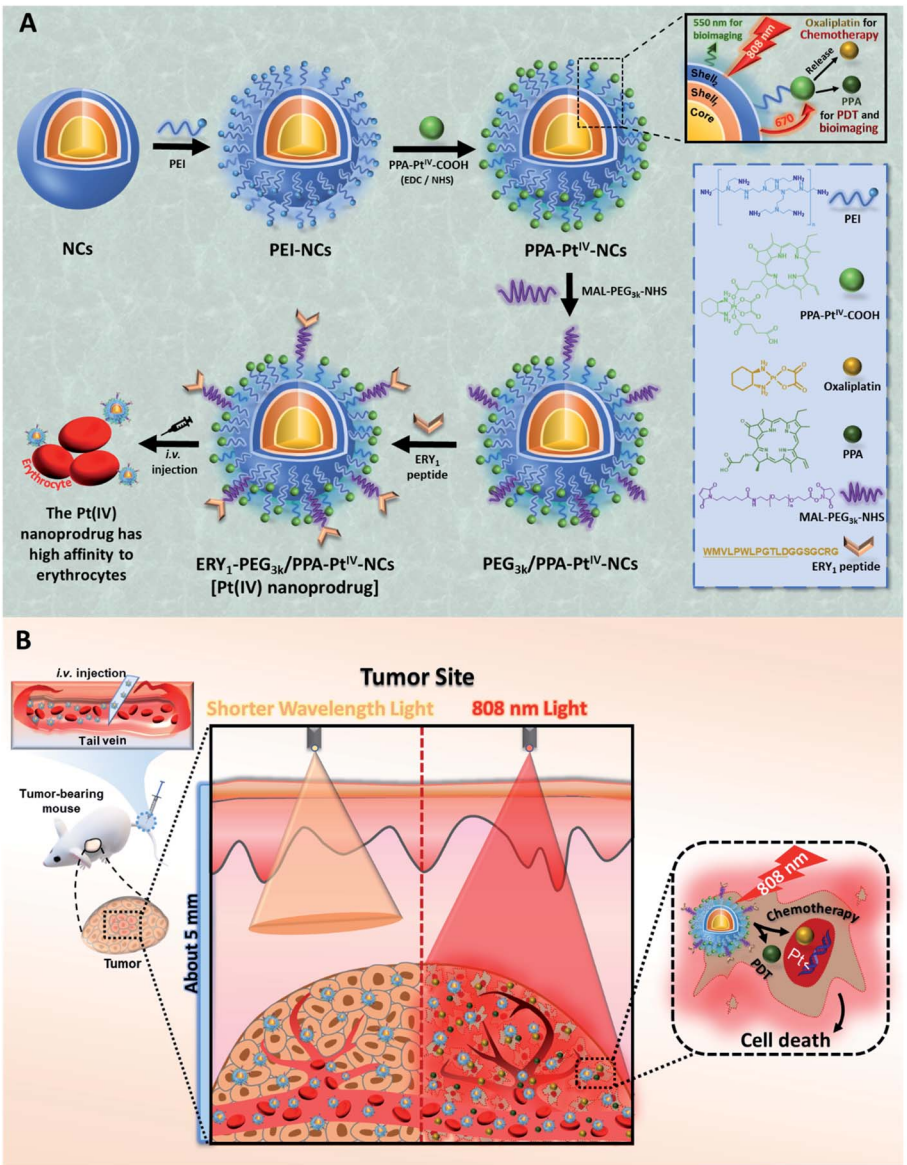

Scheme 1 Strategic illustration of the erythrocyte-delivered and NIR-photoactivatable Pt^{IV} nanoprodrug for enhanced cancer treatment. (A) Stepwise engineering of NIR-activatable ERY$_1$-PEG$_{3k}$/PPA-Pt^{IV}-NCs that anchor erythrocytes for drug delivery. (B) Schematic illustration of the Pt^{IV} nanoprodrug shuttled by erythrocytes after circulation to elicit improved chemo-photodynamic therapy upon NIR irradiation at 808 nm. NCs, dielectric nanocrystals; PEI, polyethylenimine; PPA, pyropheophorbide a; PDT, photodynamic therapy.

μM), respectively (Fig. S17†). This 20-fold increase in Pt accumulation in the presence of the nanocomplex clearly indicates the efficient delivery of the Pt^{IV} prodrug into the cancer cells. The level of Pt in the genomic DNA was subsequently measured in the cells treated with PPA-Pt^{IV}-NCs. An 8-fold increase in the level of Pt in the genomic DNA was detected after irradiation, compared to the level without irradiation (Fig. S18†). Since Pt^{IV} prodrugs can only efficiently bind to DNA after reduction to their Pt(II) species,[39] this result clearly shows the efficient photocontrollable activation of the nanocomplex in cancer cells. Furthermore, intracellular reactive oxygen species (ROS) were generated after treatment with PPA-Pt^{IV}-NCs (Fig. S19†), indicating that this nanocomplex can kill cancer cells using a mode of combined chemo-photodynamic therapy.

Next, we endeavored to functionalize the nanocomplex with an erythrocyte-binding ability to achieve our original goals. Due to the presence of additional free amino groups on the surface, a linker *O*-[*N*-(6-maleimidohexanoyl)aminoethyl]-*O*′-[3-(*N*-succinimidyloxy)-3-oxopropyl]polyethylene glycol 3000 (NHS-PEG$_{3k}$-MAL) was covalently loaded onto the surface of the nanocomplex to obtain PEG$_{3k}$/PPA-Pt^{IV}-NCs. Subsequently, the ERY$_1$ peptide was conjugated on PEG$_{3k}$/PPA-Pt^{IV}-NCs through a reaction of the thiol-reactive maleimide on the distal end of the PEG$_{3k}$ and the C-terminus cysteine residue of the peptide. ERY$_1$ is a synthetic 12-aa peptide that has strong and specific biophysical targeting of an antigen to the surface of mouse erythrocytes *in situ* through binding to glycophorin-A (GYPA).[49] The resultant Pt^{IV} nanoprodrug is designated as ERY$_1$-PEG$_{3k}$/PPA-Pt^{IV}-NCs (Scheme

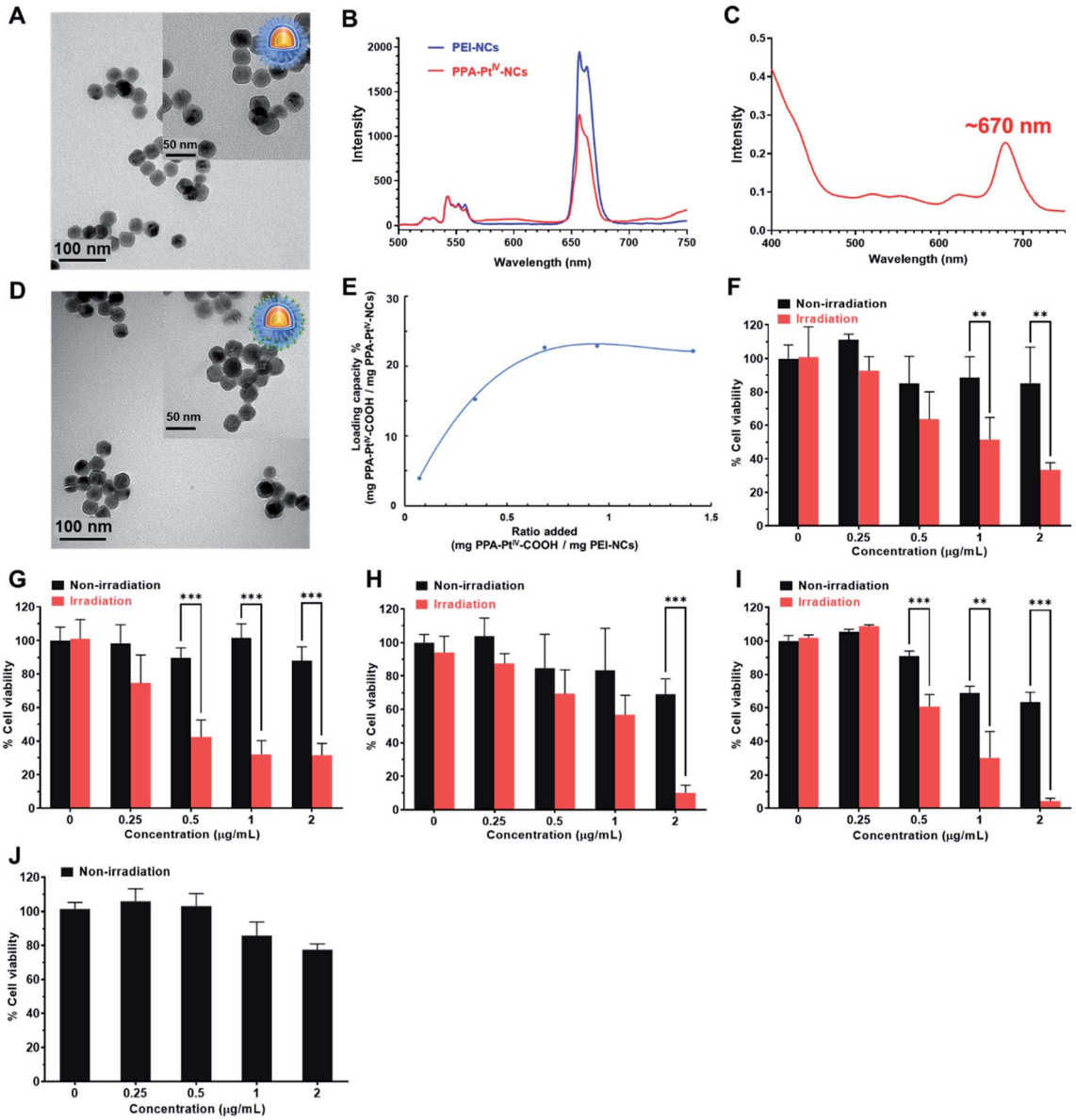

Fig. 1 Characterization and photocytotoxicities of various nanocomplexes. (A) TEM images of dielectric NCs coated with PEI (PEI-NCs). (B) Photoluminescence spectrum of aqueous solutions of PEI-NCs (blue line) and PPA-Pt^{IV}-NCs (LC% = 22%, red line) under 808 nm NIR excitation. (C) UV-Vis absorption of PPA-Pt^{IV}-COOH. Due to the overlap of the photoluminescence of NCs and the absorption of PPA-Pt^{IV}-COOH, the generated emission at 670 nm from PEI-NCs may further photoactivate the Pt^{IV} prodrug to release oxaliplatin. (D) TEM images of PPA-Pt^{IV}-NCs (22%, w/w). (E) Loading capacity (w/w) under different ratios for the reaction. The ratio is the weight of the loaded Pt^{IV} prodrug to the weight of PPA-Pt^{IV}-NCs. Phototoxicity of PPA-Pt^{IV}-NCs (22%, w/w) in (F) 4T1, (G) MCF-7, (H) A2780, (I) A2780cisR, and (J) MRC-5 cells. The cells were treated with different concentrations (0, 0.25, 0.5, 1, and 2 μg mL^{-1}) of PPA-Pt^{IV}-NCs for 2 h, followed by irradiation at 808 nm (0.5 W cm^{-2}, 5 min per well) or kept in the dark. The culture medium containing complexes was subsequently replaced by fresh medium and cultured for another 48 h. The cell viabilities of untreated cells (0 μg mL^{-1} PPA-Pt^{IV}-NCs) without irradiation were set as 100% for calculation. For TEM images, scale bars are 100 nm and 50 nm for inset images. Mean ± SD; **, p <0.01; ***, p <0.001.

1). The conjugations were confirmed by TEM, ζ potential, size distribution, and FT-IR measurements (Fig. 2A, B, and S11, Table S1†). The strong photocytotoxicity presented by ERY_1-PEG_{3k}/PPA-Pt^{IV}-NCs was also confirmed (Fig. S20†).

The stability of Pt^{IV} in the dark was further examined in fresh mouse whole blood *via* reversed-phase high-performance liquid chromatography (RP-HPLC). The nanoprodrug showed significantly increased stability compared to its corresponding small molecule. Following incubation in mouse whole blood for 9 h at 37 °C, only 28.9 ± 6.7% of PPA-Pt^{IV}-COOH remained intact. In contrast, structural integrity was retained in 71.2 ± 2.5% of PPA-Pt^{IV}-NCs under the same condition. Furthermore, ERY_1-PEG_{3k}/PPA-Pt^{IV}-NCs exhibited the highest stability in the blood, as more than 91.0 ± 2.7% of Pt^{IV} remained intact after 24 h (Fig. 2C). The calculated half-lives ($t_{1/2}$) were 4.2 ± 0.3 h, 14.3 ± 0.5 h, and 91.4 ± 15.1 h for Pt^{IV} in PPA-Pt^{IV}-COOH, PPA-Pt^{IV}-

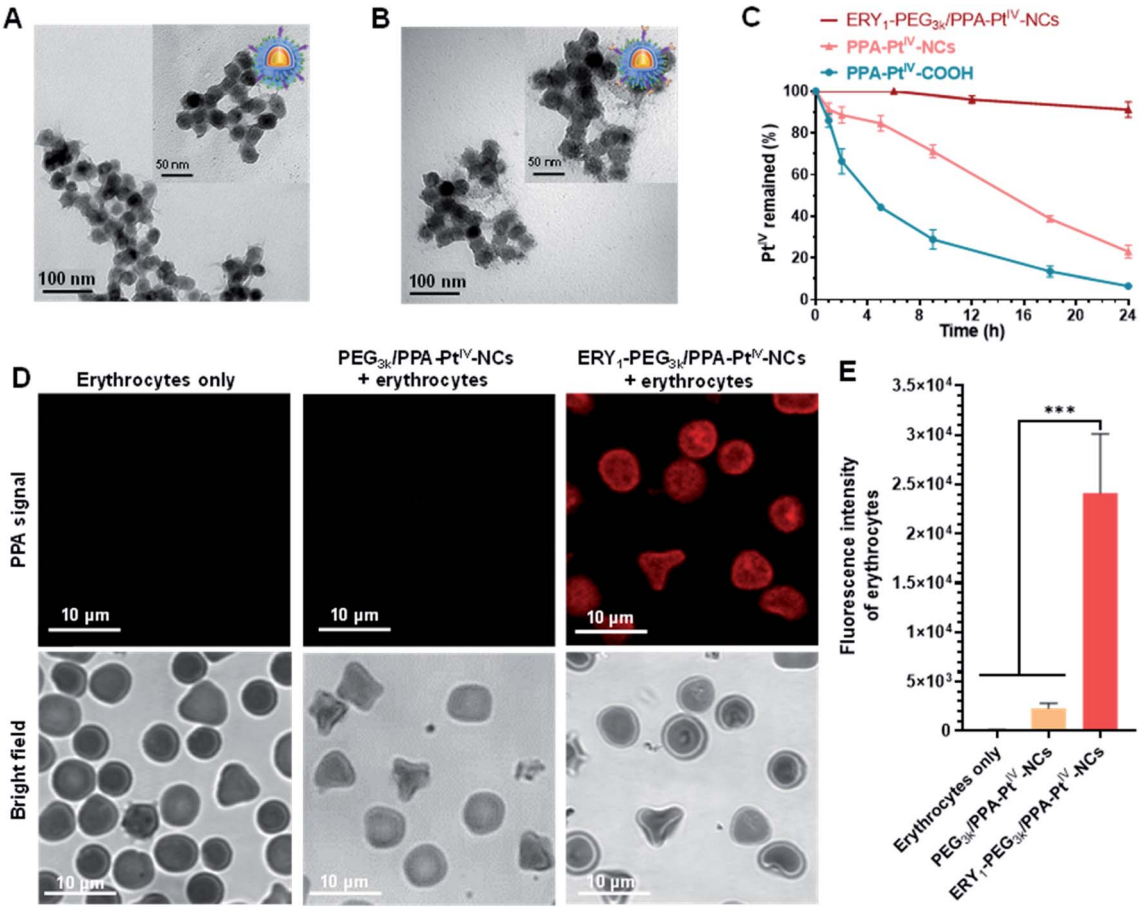

Fig. 2 Characterization, stability, and erythrocyte-binding property of the nanocomplexes. TEM images of (A) PEG_{3k}/PPA-Pt^{IV}-NCs and (B) ERY_1-PEG_{3k}/PPA-Pt^{IV}-NCs. For PEG_{3k}/PPA-Pt^{IV}-NCs, the obtained nanoparticles showed a thin layer on the surface of NCs due to the presence of the PEG linker. ERY_1-PEG_{3k}/PPA-Pt^{IV}-NCs showed a thicker layer outside the round-shaped NCs compared to PEG_{3k}/PPA-Pt^{IV}-NCs, suggesting the successful conjugation of the ERY_1 peptide. Scale bars are 100 nm for the images and 50 nm for inset images. (C) Time-dependent stability test of PPA-Pt^{IV}-NCs, PPA-Pt^{IV}-COOH, and ERY_1-PEG_{3k}/PPA-Pt^{IV}-NCs in fresh mice whole blood in the dark (37 °C). (D) Representative confocal fluorescence microscopy images of erythrocytes, erythrocytes incubated with PEG_{3k}/PPA-Pt^{IV}-NCs, and with ERY_1-PEG_{3k}/PPA-Pt^{IV}-NCs. Before the incubation and imaging, 5 mg mL^{-1} BSA was applied to all the groups to block nonspecific binding. Scale bars are 10 μm for the images. (E) Quantification of fluorescence intensity of various groups of erythrocytes *via* ImageJ according to the confocal fluorescence microscopy images. One hundred and fifty erythrocytes from each group were counted for quantification ($n = 150$). Mean ± SD; ***, $p < 0.001$.

NCs, and ERY_1-PEG_{3k}/PPA-Pt^{IV}-NCs, respectively. This result evidently suggests the improved stability of our Pt^{IV} nanoprodrug in fresh mouse blood and points to its potential for effective *in vivo* utilization.

The ability of the functionalized nanoprodrug to bind erythrocytes was subsequently confirmed using scanning electron microscopy (SEM). For PEG_{3k}/PPA-Pt^{IV}-NCs, no round nanoparticles were observed on the surface of the cells, and erythrocytes retained their physical integrity with a smooth surface (Fig. S21A and S21B†). After incubation, however, the ERY_1-conjugated Pt^{IV} nanoprodrug was able to attach to the surface of erythrocytes (Fig. S21C and S21D†). These results are attributed to the specific binding properties of the ERY_1 peptide. To better analyze the binding of the nanoprodrug to erythrocytes, confocal laser scanning microscopy (CLSM) was used for further visualization. Erythrocytes incubated with ERY_1-PEG_{3k}/PPA-Pt^{IV}-NCs showed a strong fluorescence intensity, indicating effective attachment to the surface of erythrocytes. In comparison, erythrocytes incubated with PEG_{3k}/PPA-Pt^{IV}-NCs showed a 10.5-fold weaker fluorescent signal, representing very limited binding to erythrocytes (Fig. 2D and E and S22†). Furthermore, the PPA signal detected using flow cytometry indicated that ERY_1-PEG_{3k}/PPA-Pt^{IV}-NCs were attached on the surface of erythrocytes in the greatest abundance (Fig. S23 and S24†). The ERY_1 peptide is believed to increase binding to the glycophorin A (GYPA) epitope on the erythrocyte membrane.[50] To determine whether ERY_1-PEG_{3k}/PPA-Pt^{IV}-NCs binds to erythrocytes at the GYPA epitope, a fluorescence-conjugated GYPA antibody was used. A $GYPA^+$ fluorescent signal would indicate binding of the GYPA antibody to the erythrocyte surface. In contrast, a lack of GYPA signal would indicate that the ERY_1-conjugated Pt^{IV} nanoprodrug has bound to the available GYPA docking sites on the erythrocytes, thus preventing the antibody from binding. Using this rationale, the binding efficiency of PEG_{3k}/PPA-Pt^{IV}-NCs to erythrocytes was determined to be as low as 1%, which is similar to that observed

for untreated erythrocytes. In contrast, 98% of the ERY_1-modified nanoprodrug was bound to erythrocytes *via* the GYPA site (Fig. S25†). A subsequent quantitative analysis of the Pt contents of these erythrocytes using ICP-OES yielded results consistent with the flow cytometry observations (Fig. S26†). These results clearly imply the erythrocyte-binding ability of the ERY_1-conjugated nanoprodrug *via* the GYPA epitope.

The antitumor activity and immune response generated from our nanoprodrug *in vivo* were subsequently tested. The maximum tolerated dose (MTD) was determined to be 2.5 μmol-Pt kg^{-1} in BALB/c mice for single intravenous (i.v.) injection (Fig. S27†). It is well known that small-molecule Pt drugs suffer from high clearance and short circulation time with a half-life of only a few hours.[51] Such rapid clearance limits the use of Pt drugs in cancer treatment because the drug cannot efficiently reach the target site with a certain level in a restricted period. With the advances of our Pt^{IV} nanoprodrug, the accumulation in the tumor site is expected to be improved by erythrocyte

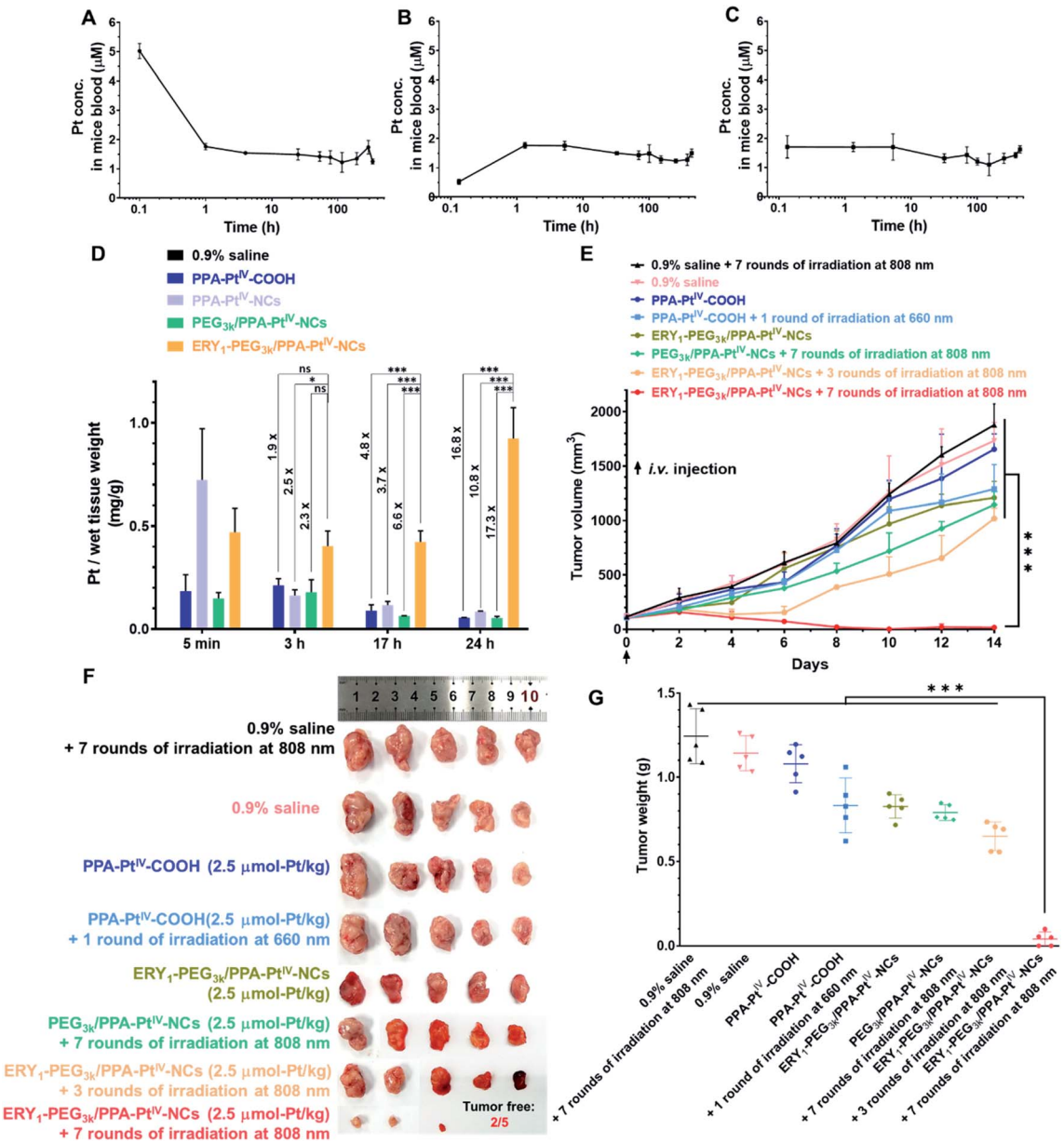

Fig. 3 Pharmacokinetic tests and anticancer evaluation in 4T1 tumor-bearing BALB/c mice after intravenous (*i.v.*) injection with various complexes. The Pt concentration curve in plasma at each time point is from single dose i.v. injection of (A) PPA-Pt^{IV}-COOH, (B) PEG_{3k}/PPA-Pt^{IV}-NCs, and (C) ERY_1-PEG_{3k}/PPA-Pt^{IV}-NCs. (D) The Pt accumulation in the tumor determined by ICP-OES at each corresponding time point indicated. (E) Anticancer activity after treatment with various complexes. The indicated complexes were i.v. injected once on Day 0 and treated with or without irradiation. Irradiation conditions: 660 nm laser (100 mW cm^{-2}) for 10 min per mouse, 808 nm laser (0.5 W cm^{-2}) for 30 min (5 min irradiation with 5 min interval) per mouse. Experimental details are described in the ESI.† (F) Photograph of excised tumors at the endpoint (Day 14) of anticancer evaluation. (G) Tumor weights of different treatment groups in the 4T1 xenograft model after the termination of anticancer evaluation. Mean ± SD; $n = 3$. *, $p < 0.05$; ***, $p < 0.001$; ns, no significance. Student's *t*-test.

shuttling during circulation in the bloodstream. To evaluate the circulation half-life in blood vessels, PPA-Pt^{IV}-COOH, PEG_{3k}/PPA-Pt^{IV}-NCs, and ERY_1-PEG_{3k}/PPA-Pt^{IV}-NCs were injected *via* the tail vein. The blood was collected by retro-orbital puncture from each anesthetized mouse at ten continuous time points. The curves of Pt concentration in the mice bloodstream indicated that the three complexes had different pharmacokinetic profiles. For the small molecule, the Pt concentration in the bloodstream decreased rapidly within the first 1 h and then declined slowly with a long terminal phase (Fig. 3A). For the PEGylated nanocomplex, a slow increase in Pt concentration was observed in the first 1 h (Fig. 3B). For the ERY_1-modified Pt^{IV} nanoprodrug, however, the Pt concentration in the blood kept at a relatively flat level once injected (Fig. 3C), suggesting a quick redistribution in the blood through its strong erythrocyte-anchoring property and subsequent circulation to the whole body. The calculated circulation $t_{1/2}$ of the small-molecule PPA-Pt^{IV}-COOH was only 0.79 h, while the erythrocyte-delivered Pt^{IV} nanoprodrug was as high as 907.76 h (Table S2†). All these data confirm that our ERY_1-functionalized Pt^{IV} nanoprodrug has significantly improved circulation time *in vivo* over the free small molecules by rapidly attaching to the erythrocytes.

Based on the *in vitro* studies and *in vivo* pharmacokinetic results, we expect that our ERY_1-functionalized Pt^{IV} nanoprodrug may have elevated accumulation in the tumor site after a prolonged circulation. To corroborate this hypothesis, a murine mammary adenocarcinoma 4T1 xenograft model was established to investigate the biodistribution of various complexes *in vivo*. As observed by a bio-imaging system, the fluorescence intensity in the tumor treated with ERY_1-PEG_{3k}/PPA-Pt^{IV}-NCs remained at a relatively high level (Fig. S28A†). This result indicates the strong accumulation of our nanoprodrug in the tumor after the elongated circulation. For clearer observation, the mice were sacrificed at different time points, and the major organs and tumors were harvested for *ex vivo* imaging. As shown from the fluorescence images of excised tissues and the corresponding fluorescence intensity, the ERY_1-functionalized nanoprodrug succeeded in accumulating in the tumor and maintaining at a high level (Fig. S28B†). To better quantify the distribution in target tissues, Pt accumulation in the tumor was analyzed by ICP-OES. After i.v. injection *via* the tail vein, the level of Pt in the tumor decreased gradually in all the test groups, except for ERY_1-PEG_{3k}/PPA-Pt^{IV}-NCs (Fig. 3D). Compared with the small-molecule or non-functionalized nanocomplex, this ERY_1-functionalized nanoprodrug shows significantly elevated accumulation in the tumor. For example, compared with PEG_{3k}/PPA-Pt^{IV}-NCs, a 6.6-fold increase in the Pt level in the tumor was observed after 17 h, and the fold increase was as high as 17.3 after 24 h. These results provide strong evidence that ERY_1-PEG_{3k}/PPA-Pt^{IV}-NCs accumulate strikingly efficiently in the tumor after circulation in the body. With hitchhiking of the nanoprodrug on erythrocytes, the Pt level increased steadily in the tumor site, which can be utilized to produce a stronger chemotherapeutic effect.

Subsequently, the *in vivo* antitumor activity of our nanoprodrug ERY_1-PEG_{3k}/PPA-Pt^{IV}-NCs was examined using a 4T1 tumor model. Tumor-bearing BALB/c mice were intravenously (i.v.) injected once with the different complexes at a dose of 2.5 μmol-Pt kg^{-1}. Three hours later, the tumors were irradiated with NIR light at different frequencies (Fig. S29†). As indicated in Fig. 3E, S30, and S31,† the control group, which was administered an equal volume of 0.9% saline, demonstrated no antitumor effects either with or without NIR irradiation. Without irradiation, the mice treated with the small molecule PPA-Pt^{IV}-COOH did not show significant tumor inhibition relative to the untreated groups; after irradiation at 660 nm, a limited anticancer effect was achieved in the group treated with the small molecule. In the group treated with ERY_1-PEG_{3k}/PPA-Pt^{IV}-NCs, weak tumor growth inhibition was observed without irradiation, which was likely due to a slow reduction of the Pt^{IV} prodrug in the nanoprodrug at the tumor site. An increased antitumor effect was observed in the mice treated with ERY_1-PEG_{3k}/PPA-Pt^{IV}-NCs after three rounds of NIR irradiation, indicating the effective photoactivation of the nanoprodrug. Notably, the strongest antitumor effect was achieved with ERY_1-PEG_{3k}/PPA-Pt^{IV}-NCs and seven rounds of irradiation. At the end of the study, the tumor volume in this group showed a significant reduction in comparison to the volumes in the other 7 groups (p <0.001). The average tumor volume was only 16.1 ± 15.4 mm^3 in the mice treated with ERY_1-PEG_{3k}/PPA-Pt^{IV}-NCs and seven rounds of NIR irradiation, which represents reduction of 98.7% and 98.6% relative to those treated with PPA-Pt^{IV}-COOH and PEG_{3k}/PPA-Pt^{IV}-NCs, respectively. More intriguingly, two of the five tumors were completely resolved in the group treated with our Pt^{IV} nanoprodrug (Fig. 3F and S32†). The lowest tumor weights were also observed in the ERY_1-PEG_{3k}/PPA-Pt^{IV}-NCs-treated group (Fig. 3G). These results are likely due to the tendency of the nanoprodrug to accumulate in the tumors after being transported by the erythrocytes, and continuous drug activation mediated by several rounds of irradiation.

Despite killing cancer cells by causing DNA damage, oxaliplatin is recently identified as an immunomodulator to enhance the response of cytotoxic T lymphocytes through ICD.[52,53] Moreover, cell debris caused by cytotoxic oxaliplatin and PDT could act as antigens to recruit intratumoral infiltration of immune cells and further strengthen cancer treatment.[13] We expect that the enhanced accumulation of the Pt^{IV} nanoprodrug can precisely and adequately induce a potent immune response to improve the cancer treatment *in vivo*. The antitumor immune response was subsequently examined by investigating the frequencies of intratumoral T cells, including $CD4^+$ ($CD3^+CD4^+$ as the marker) and $CD8^+$ ($CD3^+CD8^+$ as the marker) T cells, in collected tumors *via* flow cytometric analysis. The isolated single cells from the tumors were obtained and stained with fluorochrome-conjugated CD3, CD4, and CD8 antibodies as the T cell surface markers.[54] It is well known that effector $CD4^+$ T cells released from the lymph node could reach the tumor by blood vessels to kill tumor cells after immune stimulation.[55] Besides, $CD8^+$ T cells act as the cytotoxic agent in the front line of the tumor microenvironment.[56] Animals treated with PPA-Pt^{IV}-COOH without irradiation have 1.0% $CD4^+$ and 1.8% $CD8^+$ T lymphocytes in the tumor, similar to the untreated ones (1.0%

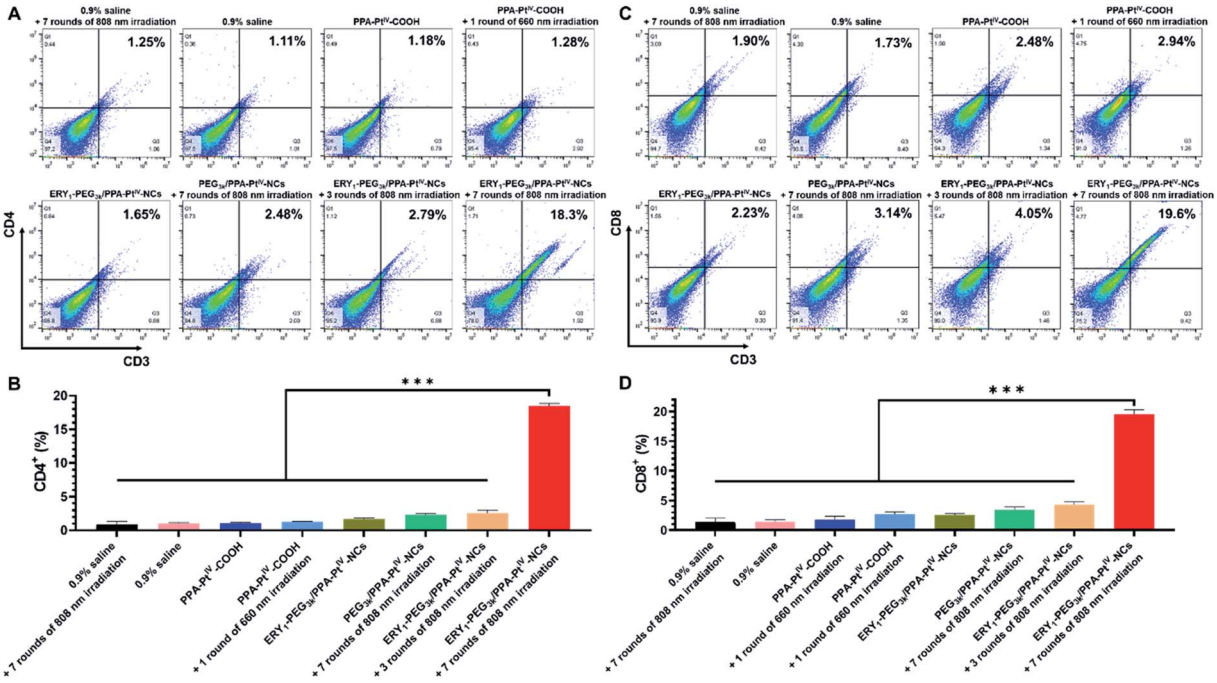

Fig. 4 Flow cytometry to quantify the populations of intratumoral T cells of the mice administered with various complexes on Day 14. (A) Representative flow cytometric analysis of the frequency of $CD4^+$ T cells in tumors (gated on $CD3^+$ and $CD4^+$). (B) Quantification of the frequency of $CD4^+$ T cells in tumors (gated on $CD3^+$ and $CD4^+$). (C) Representative flow cytometric analysis of the frequency of $CD8^+$ T cells in tumors (gated on $CD3^+$ and $CD8^+$). (D) Quantification of the frequency of $CD8^+$ T cells in tumors (gated on $CD3^+$ and $CD8^+$). The results were quantified based on three different tumors from each group. Mean ± SD, $n = 3$. ***, p <0.001. Student's t-test.

$CD4^+$ and 1.4% $CD8^+$, Fig. 4). Upon irradiation after treatment with the small molecule or PEG_{3k}/PPA-Pt^{IV}-NCs, the frequencies of $CD4^+$ and $CD8^+$ T cells did not significantly increase in the tumor, indicating that the small molecule itself and the non-functionalized nanoparticles were not strong enough to activate sufficient antitumor immune response (Fig. 4). The result could be attributed to unsatisfactory tumor accumulation capacity with only a single dose. In contrast, the mice treated with ERY_1-PEG_{3k}/PPA-Pt^{IV}-NCs after 808 nm NIR irradiation showed significantly higher frequencies of $CD4^+$ and $CD8^+$, especially when more rounds of irradiation were applied. For instance, with the treatment of our nanoprodrug, the frequencies of $CD4^+$ and $CD8^+$ T cells were 18.5% and 19.5%, which were 14.5-fold and 7.2-fold higher than those from the photoactivated small molecule, respectively. Hence, our Pt^{IV} nanoprodrug shuttled by erythrocytes exhibited a significantly enhanced synergistic immunopotentiation action compared with the small molecule or the nonfunctionalized nanoparticles alone upon single injection.

The safety of anticancer drugs is another major concern during the evaluation of antineoplastics.[57] Due to the controllable activation property of our Pt^{IV} nanoprodrug, we anticipate that the multifunctional nanoprodrug may have low damage to normal tissues. Subsequently, the bodyweight of all the treated mice was measured every other day during the observation period. Minimal variations have been observed for all the tested groups (Fig. S33†). After treatment with ERY_1-PEG_{3k}/PPA-Pt^{IV}-NCs and seven rounds of irradiation, the spleen weights recovered to the normal level (Fig. S34†). Meanwhile, blood biochemical indexes were also measured to evaluate the systemic toxicity on day 14 post-injection. The concentrations of aspartate transaminase (AST), alanine aminotransferase (ALT), creatinine, uric acid (UA), and blood urea nitrogen (BUN) had no significant alterations after treatments (Fig. S35†). Besides, no obvious change was found in all the major organs from the treatment groups through the hematoxylin and eosin (H&E) staining (Fig. S36†). Taken together, these assays verify the safety and minimal systemic toxicity of our ERY_1-PEG_{3k}/PPA-Pt^{IV}-NC nanoprodrug that displays more effective anticancer activity over the small molecule.

Conclusion

In conclusion, we have engineered an erythrocyte-delivered oxaliplatin-based Pt^{IV} nanoprodrug that can be controllably activated by NIR light for the treatment of breast cancer. Compared with the corresponding small-molecule prodrug, our nanocomplex showed significantly improved stability in the blood and could be activated effectively by NIR light to release oxaliplatin and generate ROS. The nanocomplex exhibited low toxicity in the dark but high photocytotoxicity in various cancer cells, including Pt-resistant ones. The Pt^{IV} nanoprodrug was able to bind erythrocytes strongly and specifically, and as a result, the half-life in the circulatory system improved from hours for the small molecule alone to weeks for our nanoprodrug. Consequently, we observed more than a magnitude

enhanced drug accumulation in the tumors after treatment with our nanoprodrug relative to other Pt complexes, which lacked innate erythrocyte-binding properties. In a mouse model of breast cancer, extraordinary tumor regression was achieved with just a single injected dose of our nanoprodrug under NIR irradiation, and complete tumor elimination was even observed in some cases. Additionally, increased neoantigen expression was observed in the mice treated with the Pt^{IV} nanoprodrug when compared to other drugs lacking erythrocyte-mediated delivery, and a stronger synergistic immune activation effect was observed as indicated by an increased population of cytotoxic T lymphocytes in the tumors. Overall, our Pt^{IV} nanoprodrug exhibited significantly enhanced chemotherapeutic effects as a consequence of erythrocyte-mediated delivery. Compared with conventional upconverting nanosystems loaded with diazido-Pt(IV) complexes without erythrocyte-binding properties, our nanoprodrug has apparent advantages of higher drug release efficiency, impressive stability in reducing environments, elongated circulation after i.v. injection, substantial tumor inhibition, and elevated immune response.[58,59] We believe that our bioinspired NIR-controlled Pt^{IV} nanoprodrug provides not only a paradigm to overcome the shortages of small-molecule Pt-based drugs but also an inspiring advanced drug delivery system for cancer therapy.

Data availability

All experimental supporting data and procedures are available in the ESI.†

Author contributions

G. Z. and J. S. designed the project. G. Z. and N. W. designed the experiments and wrote the manuscript. N. W. performed the Pt nanoprodrug synthesis, characterization, *in vitro* and *in vivo* tests. Q. Z., J. Z., and F. W. conducted the synthesis and characterization of PEI-UCNPs. Z. D. and Z. W. conducted the synthesis and characterization of PPA-Pt^{IV}-COOH. N. W., K. X., and P. S. carried out the animal imaging assays. X. C. and F. W. provided critical advice during the manuscript writing. All authors have given approval to the final version of the manuscript.

Conflicts of interest

There are no conflicts to declare.

Acknowledgements

We thank the Hong Kong Research Grants Council (Grant Nos CityU 11307419, 11304318, 11303320, and 11205219) and the National Natural Science Foundation of China (Grant Nos 21877092 and 22077108) for funding support. All BALB/c mice were bought from the Chinese University of Hong Kong and the City University of Hong Kong, maintained under pathogen-free conditions at the City University of Hong Kong. All animal procedures were performed following the Guidelines for Care and Use of Laboratory Animals of the City University of Hong Kong and approved by the Animal Ethics Committee of the City University of Hong Kong.

References

1 F. B. Jensen, *J. Exp. Biol.*, 2009, **212**, 3387–3393.
2 M. Moras, S. D. Lefevre and M. A. Ostuni, *Front. Physiol.*, 2017, **8**, 1076.
3 E. A. Evans, in *Methods Enzymol*, Academic Press, 1989, vol. 173, pp. 3–35.
4 I. V. Pivkin, Z. Peng, G. E. Karniadakis, P. A. Buffet, M. Dao and S. Suresh, *Proc. Natl. Acad. Sci. U. S. A.*, 2016, **113**, 7804–7809.
5 P.-A. Oldenborg, A. Zheleznyak, Y.-F. Fang, C. F. Lagenaur, H. D. Gresham and F. P. Lindberg, *Science*, 2000, **288**, 2051–2054.
6 P. Burger, P. Hilarius-Stokman, D. de Korte, T. K. van den Berg and R. van Bruggen, *Blood*, 2012, **119**, 5512–5521.
7 P. Wang, X. Li, C. Yao, W. Wang, M. Zhao, A. M. El-Toni and F. Zhang, *Biomaterials*, 2017, **125**, 90–100.
8 M. Xuan, J. Shao, J. Zhao, Q. Li, L. Dai and J. Li, *Angew. Chem., Int. Ed.*, 2018, **57**, 6049–6053.
9 G. Wan, B. Chen, L. Li, D. Wang, S. Shi, T. Zhang, Y. Wang, L. Zhang and Y. Wang, *Biomaterials*, 2018, **155**, 25–40.
10 W. M. Usman, T. C. Pham, Y. Y. Kwok, L. T. Vu, V. Ma, B. Peng, Y. S. Chan, L. Wei, S. M. Chin, A. Azad, A. B.-L. He, A. Y. H. Leung, M. Yang, N. Shyh-Chang, W. C. Cho, J. Shi and M. T. N. Le, *Nat. Commun.*, 2018, **9**, 2359.
11 Z. A. Chen, S. H. Wu, P. Chen, Y. P. Chen and C. Y. Mou, *ACS Appl. Mater. Interfaces*, 2019, **11**, 4790–4798.
12 S. Aryal, C. M. Hu, R. H. Fang, D. Dehaini, C. Carpenter, D. E. Zhang and L. Zhang, *Nanomedicine*, 2013, **8**, 1271–1280.
13 B. Ding, S. Shao, C. Yu, B. Teng, M. Wang, Z. Cheng, K. L. Wong, P. Ma and J. Lin, *Adv. Mater.*, 2018, **30**, e1802479.
14 Y. He, R. Li, H. Li, S. Zhang, W. Dai, Q. Wu, L. Jiang, Z. Zheng, S. Shen, X. Chen, Y. Zhu, J. Wang and Z. Pang, *ACS Nano*, 2019, **13**, 4148–4159.
15 C.-M. J. Hu, L. Zhang, S. Aryal, C. Cheung, R. H. Fang and L. Zhang, *Proc. Natl. Acad. Sci. U. S. A.*, 2011, **108**, 10980–10985.
16 N. Doshi, A. S. Zahr, S. Bhaskar, J. Lahann and S. Mitragotri, *Proc. Natl. Acad. Sci. U. S. A.*, 2009, **106**, 21495–21499.
17 C. H. Villa, A. C. Anselmo, S. Mitragotri and V. Muzykantov, *Adv. Drug Delivery Rev.*, 2016, **106**, 88–103.
18 W. Gao, C.-M. J. Hu, R. H. Fang, B. T. Luk, J. Su and L. Zhang, *Adv. Mater.*, 2013, **25**, 3549–3553.
19 S. Kontos, I. C. Kourtis, K. Y. Dane and J. A. Hubbell, *Proc. Natl. Acad. Sci. U. S. A.*, 2012, **110**, E60–E68.
20 J. S. Brenner, D. C. Pan, J. W. Myerson, O. A. Marcos-Contreras, C. H. Villa, P. Patel, H. Hekierski, S. Chatterjee, J.-Q. Tao, H. Parhiz, K. Bhamidipati, T. G. Uhler, E. D. Hood, R. Y. Kiseleva, V. S. Shuvaev, T. Shuvaeva, M. Khoshnejad, I. Johnston, J. V. Gregory, J. Lahann, T. Wang, E. Cantu, W. M. Armstead, S. Mitragotri and V. Muzykantov, *Nat. Commun.*, 2018, **9**, 2684.

21 Z. Chai, D. Ran, L. Lu, C. Zhan, H. Ruan, X. Hu, C. Xie, K. Jiang, J. Li, J. Zhou, J. Wang, Y. Zhang, R. H. Fang, L. Zhang and W. Lu, *ACS Nano*, 2019, **13**, 5591–5601.
22 T. C. Johnstone, K. Suntharalingam and S. J. Lippard, *Chem. Rev.*, 2016, **116**, 3436–3486.
23 Z. Wang, Z. Deng and G. Zhu, *Dalton Trans.*, 2019, **48**, 2536–2544.
24 N. Wang, Z. Wang, Z. Xu, X. Chen and G. Zhu, *Angew. Chem., Int. Ed.*, 2018, **57**, 3426–3430.
25 C. Imberti, P. Zhang, H. Huang and P. J. Sadler, *Angew. Chem., Int. Ed.*, 2020, **59**, 61–73.
26 L. Kelland, *Nat. Rev. Cancer*, 2007, **7**, 573–584.
27 C. A. Rabik and M. E. Dolan, *Cancer Treat. Rev.*, 2007, **33**, 9–23.
28 X. Wang, X. Wang, S. Jin, N. Muhammad and Z. Guo, *Chem. Rev.*, 2019, **119**, 1138–1192.
29 D. Gibson, *Dalton Trans.*, 2016, **45**, 12983–12991.
30 E. Wexselblatt and D. Gibson, *J. Inorg. Biochem.*, 2012, **117**, 220–229.
31 Z. Xu, Z. Wang, Z. Deng and G. Zhu, *Coord. Chem. Rev.*, 2021, **442**, 213991.
32 V. E. Y. Lee, C. F. Chin and W. H. Ang, *Dalton Trans.*, 2019, **48**, 7388–7393.
33 H. Shi, C. Imberti, H. Huang, I. Hands-Portman and P. J. Sadler, *Chem. Commun.*, 2020, **56**, 2320–2323.
34 G. Thiabaud, R. McCall, G. He, J. F. Arambula, Z. H. Siddik and J. L. Sessler, *Angew. Chem., Int. Ed.*, 2016, **55**, 12626–12631.
35 J. F. Arambula and J. L. Sessler, *Chem*, 2020, **6**, 1634–1651.
36 C. Lange and P. J. Bednarski, *Int. J. Mol. Sci.*, 2018, **19**, 3183.
37 F. S. M. Patrick, J. Bednarski and P. J. Sadler, *Anticancer Agents Med. Chem.*, 2007, **7**, 75–93.
38 Z. Wang, N. Wang, S.-C. Cheng, K. Xu, Z. Deng, S. Chen, Z. Xu, K. Xie, M.-K. Tse, P. Shi, H. Hirao, C.-C. Ko and G. Zhu, *Chem*, 2019, **5**, 3151–3165.
39 Z. Deng, N. Wang, Y. Liu, Z. Xu, Z. Wang, T.-C. Lau and G. Zhu, *J. Am. Chem. Soc.*, 2020, **142**, 7803–7812.
40 A. Tesniere, F. Schlemmer, V. Boige, O. Kepp, I. Martins, F. Ghiringhelli, L. Aymeric, M. Michaud, L. Apetoh, L. Barault, J. Mendiboure, J. P. Pignon, V. Jooste, P. van Endert, M. Ducreux, L. Zitvogel, F. Piard and G. Kroemer, *Oncogene*, 2010, **29**, 482–491.
41 S. V. Hato, A. Khong, I. J. M. de Vries and W. J. Lesterhuis, *Clin. Cancer Res.*, 2014, **20**, 2831–2837.
42 L. Galluzzi, J. Humeau, A. Buqué, L. Zitvogel and G. Kroemer, *Nat. Rev. Clin. Oncol.*, 2020, **17**, 725–741.
43 F. Ai, Q. Ju, X. Zhang, X. Chen, F. Wang and G. Zhu, *Sci. Rep.*, 2015, **5**, 10785.
44 S. Kontos and J. A. Hubbell, *Mol. Pharm.*, 2010, **7**, 2141–2147.
45 D. B. Keskin, A. J. Anandappa, J. Sun, I. Tirosh, N. D. Mathewson, S. Li, G. Oliveira, A. Giobbie-Hurder, K. Felt, E. Gjini, S. A. Shukla, Z. Hu, L. Li, P. M. Le, R. L. Allesøe, A. R. Richman, M. S. Kowalczyk, S. Abdelrahman, J. E. Geduldig, S. Charbonneau, K. Pelton, J. B. Iorgulescu, L. Elagina, W. Zhang, O. Olive, C. McCluskey, L. R. Olsen, J. Stevens, W. J. Lane, A. M. Salazar, H. Daley, P. Y. Wen, E. A. Chiocca, M. Harden, N. J. Lennon, S. Gabriel, G. Getz, E. S. Lander, A. Regev, J. Ritz, D. Neuberg, S. J. Rodig, K. L. Ligon, M. L. Suvà, K. W. Wucherpfennig, N. Hacohen, E. F. Fritsch, K. J. Livak, P. A. Ott, C. J. Wu and D. A. Reardon, *Nature*, 2019, **565**, 234–239.
46 W. Kong, T. Sun, B. Chen, X. Chen, F. Ai, X. Zhu, M. Li, W. Zhang, G. Zhu and F. Wang, *Inorg. Chem.*, 2017, **56**, 872–877.
47 H. Wen, H. Zhu, X. Chen, T. F. Hung, B. Wang, G. Zhu, S. F. Yu and F. Wang, *Angew. Chem., Int. Ed.*, 2013, **52**, 13419–13423.
48 K. R. Weishaupt, C. J. Gomer and T. J. Dougherty, *Cancer Res.*, 1976, **36**, 2326–2329.
49 K. Sahoo, R. S. Koralege, N. Flynn, S. Koteeswaran, P. Clark, S. Hartson, J. Liu, J. D. Ramsey, C. Pope and A. Ranjan, *Pharm. Res.*, 2016, **33**, 1191–1203.
50 S. Kontos, I. C. Kourtis, K. Y. Dane and J. A. Hubbell, *Proc. Natl. Acad. Sci. U. S. A.*, 2013, **110**, E60–E68.
51 X.-J. Liang, C. Chen, Y. Zhao and P. C. Wang, *Methods Mol. Biol.*, 2010, **596**, 467–488.
52 D. Wang and S. J. Lippard, *Nat. Rev. Drug Discovery*, 2005, **4**, 307–320.
53 W. M. Liu, D. W. Fowler, P. Smith and A. G. Dalgleish, *Br. J. Cancer*, 2010, **102**, 115–123.
54 M. S. Goldberg, *Nat. Rev. Cancer*, 2019, **19**, 587–602.
55 M. Pepper and M. K. Jenkins, *Nat. Immunol.*, 2011, **12**, 467–471.
56 N. Zhang and M. J. Bevan, *Immunity*, 2011, **35**, 161–168.
57 L. He, T. Nie, X. Xia, T. Liu, Y. Huang, X. Wang and T. Chen, *Adv. Funct. Mater.*, 2019, **29**, 1901240.
58 Y. Dai, H. Xiao, J. Liu, Q. Yuan, P. a. Ma, D. Yang, C. Li, Z. Cheng, Z. Hou, P. Yang and J. Lin, *J. Am. Chem. Soc.*, 2013, **135**, 18920–18929.
59 Y. Min, J. Li, F. Liu, E. K. Yeow and B. Xing, *Angew. Chem., Int. Ed.*, 2014, **4**, 1012–1016.